WIDEBAND AIR-COUPLED PZT PIEZOELECTRIC MICROMACHINED ULTRASONIC TRANSDUCER THROUGH DC BIAS TUNING

Yuri Kusano[1], Qi Wang[1], Ryan Q. Rudy[2], Ronald G. Polcawich[2], and David A. Horsley[1]
[1]University of California, Davis, USA
[2]US Army Research Laboratory, USA

ABSTRACT

Wide bandwidth for an air-coupled piezoelectric micromachined transducer (PMUT) is important to achieve short pulse transmission and reception in pulse-echo imaging with high axial resolution. Here, we report experimental results on an air-coupled PMUT with high displacement sensitivity up to 5500 nm/V, high 3 dB bandwidth of 20.3 kHz, and correspondingly short transmission time of 0.05 ms, achieved through dc bias tuning. The dc bias controls the polarization and intrinsic stress of the piezoelectric layer, tuning frequencies of two closely spaced resonance modes of the ribbon-shaped PMUT. The modes nearly overlapped when applying small dc bias around ±5 V, enabling wideband and short pulse transmission.

INTRODUCTION

Ultrasonic transducers have been widely used in various applications including imaging, range-finding, nondestructive testing, flow sensing, and gesture recognition. Micromachined ultrasonic transducers (MUTs) based on MEMS technology have many advantages including miniature size, low cost, simple fabrication, ability to create 1-D and 2-D array structures, and easy integration with supporting electronics. For one type of MUT, the well-known capacitive MUT (CMUT), output pressure depends on the excitation voltage and the inverse of the capacitor gap. Since the acoustic impedance of air is much lower than that of water, air-coupled CMUTs requires large capacitor gaps and high bias voltages of nearly 150 V [1]. CMUTs with vented cavities were reported to improve the fractional bandwidth up to 36% by biasing at 250 V [2]. In contrast, piezoelectric MUTs (PMUTs) [3] can be utilized without high bias voltages, resulting in simpler electronic interfaces. Taking advantage of improved availability of high-quality piezoelectric films,

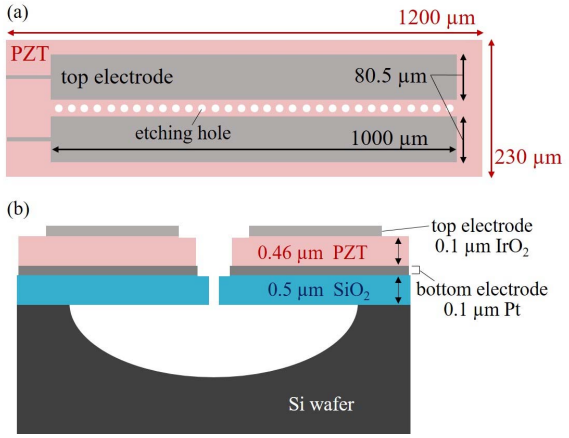

Figure 1: *Schematic (a) top view (b) cross-section of the air-coupled PZT PMUT.*

PMUTs have recently been demonstrated for many applications including range-finding [4], low-power 3-D ultrasonic imaging [5], and ultrasonic finger print sensors [6]. Among many piezoelectric MEMS devices, lead zirconate titanate (PZT) and aluminum nitride (AlN) are the two most highly used piezoelectric materials. Here, we present a PMUT using PZT, which has 10 times higher piezoelectric coefficient $e_{31,f}$ and higher transmitting efficiency than those of AlN.

In order to achieve high axial resolution in pulse-echo imaging, wide bandwidth is required for enabling a short pulse transmission to resolve objects that are closely spaced. The transmission time corresponds to the ring-down time which is scalable by the time constant of its exponential decay. The time constant is inversely proportional to the resonant frequency and proportional to the quality factor Q that corresponds to the bandwidth. Thus, the wider bandwidth, low Q in other words, results in a shorter decay time constant.

Fluid-coupled PMUTs used at high resonance frequencies (>5 MHz) often have high bandwidth (>30%), because fluid damping is high compared to air damping, and the higher speed of sound in fluid means the size of the PMUT is large relative to the transmitted wavelength. These factors allow efficient coupling for immersed PMUTs [7]. On the contrary, PMUTs operating in air require lower frequencies (<1 MHz) and are usually smaller than the wavelength (λ = 1.9 mm at 175 kHz), resulting in poor coupling and low bandwidth (1% - 5%) [8]. An air-coupled PMUT with 10% bandwidth was reported [9], but required a Helmholtz resonant tube etched into the backside of MUT to achieve this result. In this paper, we demonstrate a wideband air-coupled PMUT with resonance frequency at 175 kHz that achieves 12% bandwidth without the need for a Helmholtz resonator.

DESIGN AND FABRICATION

A schematic top view and cross-section including dimensions and layer thicknesses of each layer of a 1200 µm × 230 µm ribbon-shaped PMUT is shown in Fig. 1. The PMUT was designed with a rectangular membrane to reduce the frequency difference between adjacent working modes, (1,1) and (1,3) vibration modes [10].

The fabrication process starts with deposition of the PZT and electrode stack, Fig. 2(a). Table 1 lists the elastic modulus and layer thicknesses of the materials in the device. To begin, a 500 nm thick thermal silicon dioxide layer is grown in a tube furnace. Titanium is sputtered with a thickness of 30 nm and oxidized in a furnace to create titanium dioxide which creates a good template for the subsequently sputtered (111) textured platinum electrode with a thickness of 100 nm [11]. The oriented platinum forms a templating layer for a 475 nm thick chemical-solution deposited (001) textured PZT film with a Zr/Ti

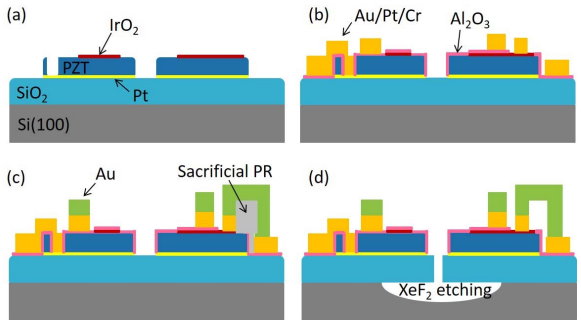

Figure 2: Fabrication process flow: deposition and patterning of (a) PZT and electrodes, (b) Al_2O_3 and Au/Pt/Cr, (c) sacrificial photoresist and thick Au layer, (d) photoresist removal and Si release.

TABLE I
YOUNG'S MODULUS AND LAYER THICKNESSES OF PMUT DEVICE

Material	YOUNG'S MODULUS [GPA]	Approximate Thickness [nm]
IrO_2	290 [13]	100
PZT 52/48	60.5 [14]	475
Pt	182 [14]	100
SiO_2	72.3 [14]	500

ratio of 52/48 [12]. The PZT is then capped with a 100 nm thick iridium oxide electrode that is sputter deposited and furnace annealed in oxygen at 650°C for 30 minutes. Next, the actuator stack is patterned using three argon ion milling steps. In the first etch, the iridium oxide is patterned to define the top electrode of the device. The second etch removes the PZT and bottom platinum from the field stopping on the silicon dioxide layer. The bottom electrode is accessed by a third ion mill step followed by a PZT wet-etch using a combination of HCl:HF:H_2O (120:1:240) to remove any residual PZT. The wafers are annealed at 500°C in an oxygen environment to mitigate any hydrogen damage from the ion milling steps.

With the actuator stack patterned, a tri-layer Au/Pt/Cr (730nm/20nm/20nm) is deposited using electron beam evaporation and patterned via liftoff, Fig. 2(b). This gold layer is used for contact pads for electrical probe testing. The silicon dioxide layer is then patterned by reactive ion etching to define the etch holes for release. Next, a sacrificial photoresist layer is defined, and a 2000 nm thick gold layer is deposited via electron beam evaporation and liftoff, Fig. 2(c). This gold layer bridges from the top electrode to the silicon dioxide in the field without shorting the electrodes in order to reduce parasitic capacitance. The sacrificial photoresist layer is removed with an oxygen plasma and the wafer is then exposed to XeF_2, which isotropically etches the underlying silicon, releasing the device, Fig. 2(d).

Fig. 3 shows the SEM image of top view and cross-section of the air-coupled PZT PMUT. The PMUT membrane was released from the front side of the wafer using XeF_2 by etching Si layer through 2 µm etching holes. Since it is difficult to conduct timed etching precisely, the resonance frequency shifts due to the XeF_2 overetch. Thick metal anchors are known to function as additional mechanical supports and reduce the frequency shift [10]. In

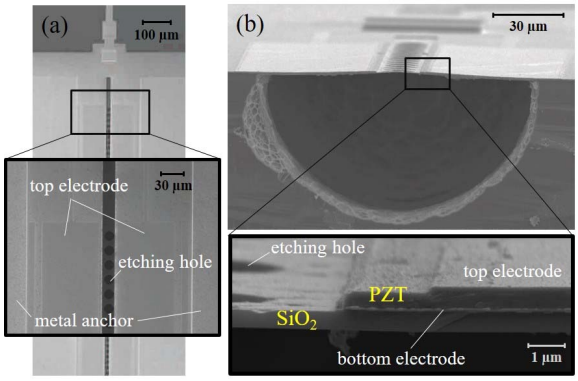

Figure 3: SEM (a) top view (b) cross-section image of the air-coupled PZT PMUT.

this work, 2 µm thick gold anchors were designed for the air-coupled PZT PMUT shown in Fig. 3(a). The breakdown voltage of the PZT film was measured to be 35V, corresponding to a breakdown field of 760 kV/cm.

RESULTS

The frequency response of the PMUT in air was measured via laser Doppler vibrometer (LDV) showing the presence of two vibration modes with closely spaced natural frequencies near 175 kHz. A dc bias voltage applied to pole the PZT layer creates in-plane piezoelectric stress that enables the frequencies of the two modes to be tuned. As the dc bias voltage was varied between ±10 V, a significant change in the resonant frequencies, displacement sensitivities, and 3 dB bandwidth were clearly observed for the two resonance modes.

In Fig. 4, the frequency response of the two resonance modes with dc bias voltages of 0 V, +6 V, +10 V respectively are shown. The two modes independently have 2.4 kHz bandwidth with displacement sensitivity of approximately 1000 nm/V with small ac voltage (-10 dBm) and without any dc bias voltage. As a result of increasing the dc bias to +6 V, the highest 3 dB bandwidth of 20.3 kHz with displacement sensitivity of 5500 nm/V were observed.

While the measured resonant frequency of the first

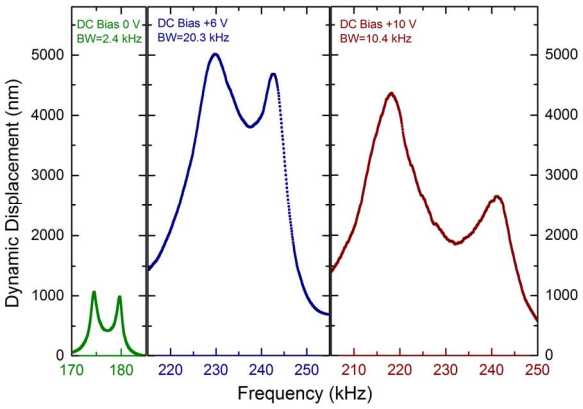

Figure 4: Frequency response measured via LDV in air with dc bias voltages of 0 V, +6 V, and +10 V respectively.

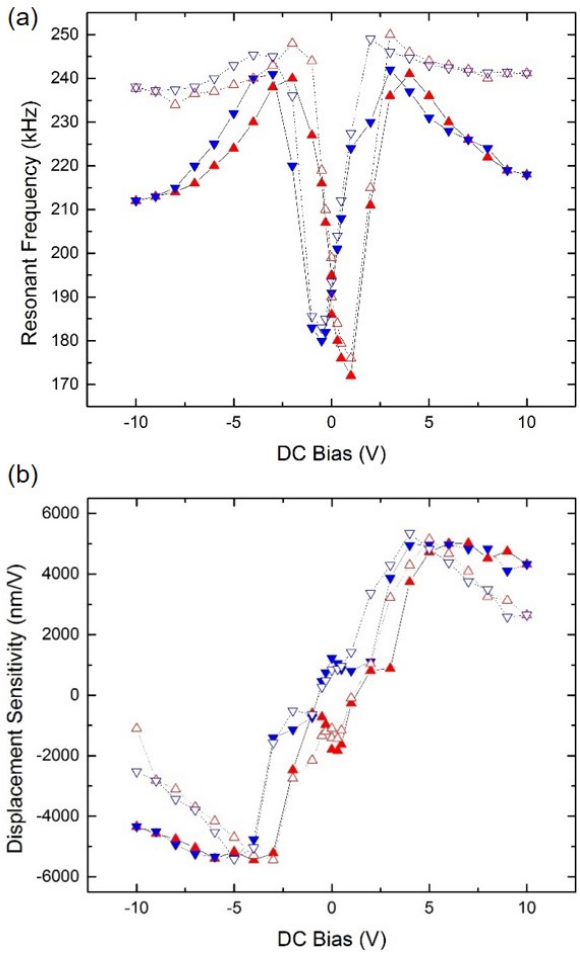

Figure 5: Dependence of (a) PMUT resonant frequency and (b) displacement sensitivity at resonance of the 1st peak (▲▼) and the 2nd peak (△ ▽) on dc bias tuning.

mode was 175 kHz without dc bias. For a rectangular membrane clamped at all four boundaries, the fundamental resonance frequency f_{00} was calculated referring [15]:

$$f_{00} = \frac{\pi}{2a^2}\sqrt{\frac{D}{\rho}\cdot\frac{K}{N}} \quad (1)$$

where D is the flexural rigidity of the plate and ρ is the area mass density. For multi-layer membrane as in this case, the D and ρ are the average values weighted by the layer thicknesses. $N = 2.25$ is a constant and K is given by the following equation:

$$K = 12 + 8\left(\frac{a}{b}\right)^2 + 12\left(\frac{a}{b}\right)^4 \quad (2)$$

where a and b are the dimensions of the membrane (a>>b). Here, we used a = 1200 µm and b = 230 µm from the actual membrane size, resulting in f_{00} = 183 kHz, which agrees with the experimental result of f_{00} = 175 kHz. Fig. 5 shows the dependence of the PMUT resonant frequency and displacement sensitivity when tuning the dc bias voltage between -10 V and +10 V. Color-filled triangles correspond to the first resonance mode and open triangles correspond to the second mode observed. In addition, upward pointing triangles present the points when sweeping up from -10 V to +10 V, while downward pointing triangles present the points when sweeping down

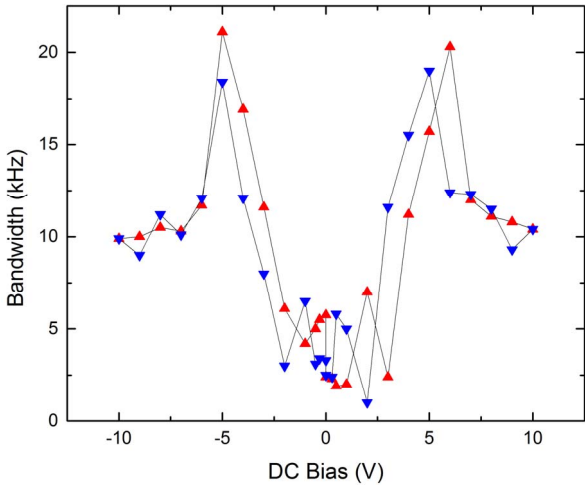

Figure 6: Dependence of the PMUT 3 dB bandwidth on dc bias tuning.

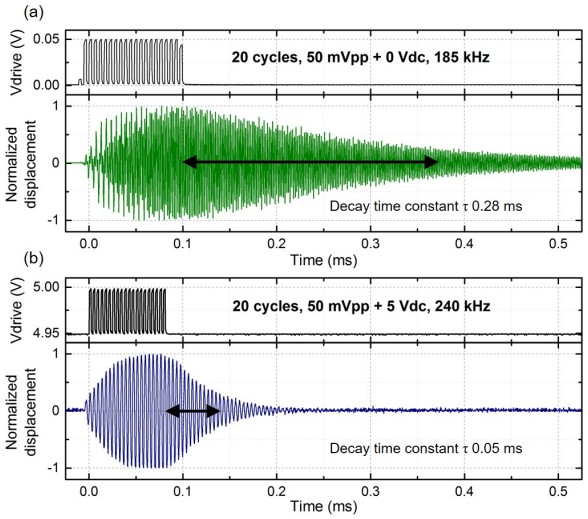

Figure 7: Time response of the PMUT driven by 20 cycles pulse V_{drive} (a) at 185 kHz without dc bias and (b) at 240 kHz with +5V dc bias.

from +10 V to -10 V.

The frequencies of the two modes are nearly overlapping with certain dc bias voltages applied, especially -5 V / +6 V while increasing and -5 V / +5 V while decreasing. From the same measurement results, the dependence of the 3 dB bandwidth on various dc bias was analyzed shown in Fig. 6. Wide 3 dB bandwidth above 20 kHz was achieved with dc bias of near ±5 V when the two closely-spaced modes have overlapping bandwidths. For other dc bias voltages, the 3 dB bandwidth was only few kHz to 10 kHz since two peaks were apart and only the first resonance mode was taken into account. Compared to the non-biased condition, 5x greater displacement sensitivity and 8.5x greater 3dB bandwidth were demonstrated through dc bias tuning.

At the bias conditions where the bandwidth is maximum, the PMUT is capable of transmitting shorter pulses for pulse-echo measurement. The time response in air was demonstrated from pulsed ring-down measurement via LDV. The PMUT was excited using a function

generator with a 50 mV peak-to-peak 20-cycle square wave at the resonant frequencies for the two different dc bias conditions, 0 V and +5 V. In both cases, unipolar drive voltages were used to prevent repoling of the PZT. Fig. 7(a) shows the driving voltage of the pulse trains, and the rise and ring-down of the PMUT transmission, without applying dc bias using the resonant frequency of 185 kHz. Fig. 7(b) shows the result with applying +5 V dc bias using the resonant frequency of 240 kHz. The frequency of the driving pulse train was increased from 185 kHz to 240 kHz because the resonance frequency of the PMUT shifted due to the dc bias applied as it was shown in Fig. 5(a).

Comparing the two ringdown plots, the decay time constant τ decreases from 0.28 ms to 0.05 ms. The approximately five-fold reduction in decay time is equal to the increase in the bandwidth, from roughly 4 kHz at 0 V bias, to 20 kHz at +5 V bias. The minimum pulse transmission time is approximately $4\tau = 0.2$ ms. In pulse-echo measurements, the first echoes that can be received must arrive later than the end of pulse transmission. Therefore, this time defines the minimum range for pulse-echo measurements, $r_{min} = 4\tau c/2 = 3.4$ cm at +5 V bias, compared to a minimum range of 19 cm at 0 V bias.

CONCLUSION

We have presented a method to increase bandwidth and reduce transmission time of air-coupled PZT PMUTs. Through dc bias tuning at ±5 V, where the piezoelectric coefficient $e_{31,f}$ at its maximum, two adjacent resonance modes almost overlapped resulting in 5x displacement sensitivity and 8.5x 3 dB bandwidth compared to when no dc bias is applied. Consequently, the time-response measurement results showed that decay time constant of the pulse transmission significantly reduced to 0.05 ms from 0.28 ms by adding +5 V dc bias to the driving voltage. The proposed dc bias tuning of the PMUT achieving wideband and short pulse demonstrated a good potential in enabling high resolution imaging for in air operation.

ACKNOWLEDGEMENTS

The authors would like to thank Brian Power and Joel Martin of the US Army Research Laboratory (ARL), Steven Isaacson of General Technical Services, and Berkeley Sensor and Actuator Center (BSAC) Industrial Members for financial support.

REFERENCES

[1] I. O. Wygant, M. Kupnik, J. C. Windsor, W. M. Wright, M. S. Wochner, G. G. Yaralioglu, M. F. Hamilton, and B. T. Khuri-Yakub, "50 kHz capacitive micromachined ultrasonic transducers for generation of highly directional sound with parametric arrays," *IEEE Trans. Ultrason. Ferroelectr. Freq. Control*, vol. 56, pp. 193–203, 2009.

[2] N. Apte, P. Kwan Kyu, A. Nikoozadeh, and B. T. Khuri-Yakub, "Bandwidth and sensitivity optimization in CMUTs for airborne applications," in *IEEE Intl Ultrasonics Symposium*, 2014, pp. 166-169.

[3] P. Muralt and J. Baborowski, "Micromachined Ultrasonic Transducers and Acoustic Sensors Based on Piezoelectric Thin Films," *Journal of Electroceramics*, vol. 12, pp. 101–108, 2004.

[4] R. J. Przybyla, S. E. Shelton, A. Guedes, I. I. Izyumin, M. H. Kline, D. A. Horsley, and B. E. Boser, "In-Air Rangefinding With an AlN Piezoelectric Micromachined Ultrasound Transducer," *IEEE Sensors Journal,* vol. 11, pp. 2690-2697, 2011.

[5] R. J. Przybyla, H. Y. Tang, A. Guedes, S. E. Shelton, D. A. Horsley, and B. E. Boser, "3D Ultrasonic Rangefinder on a Chip," *IEEE J. Solid-State Circuits*, vol. 50, pp. 320–334, 2015.

[6] Y. Lu, H. Y. Tang, S. Fung, Q. Wang, J. M. Tsai, M. Daneman, B. E. Boser, and D. A. Horsley, "Ultrasonic fingerprint sensor using a piezoelectric micromachined ultrasonic transducer array integrated with complementary metal oxide semiconductor electronics," *Appl. Phys. Lett.*, vol. 106, no. 26, p. 263503, 2015.

[7] Y. Lu, H. Y. Tang, S. Fung, B. E. Boser, and D. A Horsley, "Pulse-Echo Ultrasound Imaging Using an AlN Piezoelectric Micromachined Ultrasonic Transducer Array with Transmit Beam-Forming," *J. Microelectromechanical Systems*, vol. 25, pp. 179–187, 2014.

[8] M. D. Williams, B. A. Griffin, T. N. Reagan, J. R. Underbrink, and M. Sheplak, "An AlN MEMS piezoelectric microphone for aeroacoustic applications," *J. Microelectromechanical Systems*, vol. 21, pp. 270–283, 2012.

[9] S. Shelton, O. Rozen, A. Guedes, R. Przybyla, B. Boser, and D. A. Horsley, "Improved acoustic coupling of air-coupled micromachined ultrasonic transducers," in *27th IEEE Intl Conf on MEMS*, 2014, pp. 753-756.

[10] Y. Lu, O. Rozen, H. Y. Tang, G. L. Smith, S. Fung, B. E. Boser, R. G. Polcawich, and D. A. Horsley, "Broadband piezoelectric micromachined ultrasonic transducers based on dual resonance modes," in *28th IEEE Intl Conf on MEMS*, 2015, pp. 146-149.

[11] D. M. Potrepka, G. R. Fox, L. M. Sanchez, and R. G. Polcawich, "Pt/TiO2 Growth Templates for Enhanced PZT films and MEMS Devices," *MRS Proc.*, vol. 1299, pp. 67–72, 2011.

[12] L. M. Sanchez, D. M. Potrepka, G. R. Fox, I. Takeuchi, K. Wang, L. A. Bendersky, and R. G. Polcawich, "Optimization of PbTiO3 seed layers and Pt metallization for PZT-based piezoMEMS actuators," *J. Mater. Res.*, vol. 28, no. 14, pp. 1920–1931, 2013.

[13] Y. Li and Z. Zeng, "Elastic properties of transition metal dioxides: XO 2 (X=Ru, Rh, Os, Ir)," *Int. J. Mod. Phys. C,* vol. 19, no. 8, pp. 1269–1275, 2013.

[14] S. Yagnamurthy, I. Chasiotis, J. Lambros, R. G. Polcawich, J. S. Pulskamp, and M. Dubey, "Mechanical and ferroelectric behavior of PZT-based thin films," *J. Microelectromechanical Systems*, vol. 20, pp. 1250–1258, 2011.

[15] A. W. Leissa, *Vibration of plates*, NASA SP-160, 1969.

CONTACT

*Y. Kusano, tel: +1-530-979-4330;
ykusano@ucdavis.edu